Delay-based Input Shaping and Feedforward Design for Dual Closed-Loop Control Architectures Integrating Active Damping

Natu, A.M.; HosseinNia, S.H.

DOI
10.1016/j.ifacol.2025.10.166

Publication date
2025

Document Version
Final published version

Published in
IFAC-PapersOnline

Available online at www.sciencedirect.com

ScienceDirect

IFAC PapersOnline CONFERENCE PAPER ARCHIVE

IFAC PapersOnLine 59-17 (2025) 215–220

Delay-based Input Shaping and Feedforward Design for Dual Closed-Loop Control Architectures Integrating Active Damping ⋆

A.M. Natu * **S.H. HosseinNia** *

* *Department of Precision and Microsystems Engineering, Delft University of Technology, Mekelweg 2, 2628 CD Delft, The Netherlands (e-mail: a.m.natu@tudelft.nl; s.h.hosseinniakani@tudelft.nl)*

Abstract: In nanopositioning systems, the control bandwidth is frequently limited due to the presence of lightly damped resonant dynamics. Active Damping Control is typically integrated with tracking control within an inner-loop configuration to mitigate dominant resonant dynamics and enable higher bandwidths. The paper discusses that, in such architectures, feedforward control based on plant dynamics inversion is insufficient to achieve the intended feedforward objectives. In response to this limitation, the study introduces a delay-based input shaping and feedforward framework combined with a dual closed-loop feedback control system that includes active damping. The feedforward filter, derived from partial inner closed-loop dynamics inversion, facilitates precise, delayed tracking of reference signals. This configuration implements a unity-gain shaping filter, effectively reducing tracking feedback errors caused by reference inputs. Furthermore, the study presents a simulated example employing a simplified dynamic model of an industrial nanopositioning system to demonstrate enhancements in closed-loop periodic tracking performance through the proposed feedforward and input-shaping methodology.

Keywords: Feedforward Control, Input Shaping, Delay, Non-Minimum Phase, Active Damping, Resonant Controller, Nanopositioning, Model Inverse

1. INTRODUCTION

Nanopositioning systems are used for high-resolution positioning applications, such as imaging using atomic force microscopes (AFMs) (Fleming and Leang (2014)) or nanofabrication technologies such as force lithography, nanografting, etc. (Shan and Leang (2013)). These systems typically use piezoelectric stack actuators to generate substantial forces and high stiffness and maintain significant bandwidth and resolution. The design includes parallel flexures to guide the platform, ensuring backlash-free and frictionless operation. Nanopositioning systems often track repetitive or user-defined trajectories in various applications. For example, fast imaging is crucial for investigating the dynamics of biological samples or enhancing the throughput of nanofabrication processes, necessitating a rapid response to these reference inputs. Sensor-based feedback control systems are implemented to meet demands for enhanced speed and subnanometer resolution and ensure good reference tracking by mitigating errors from system dynamics or external disturbances (Devasia et al. (2007)).

Traditionally, simple proportional-integral (PI) controllers have predominantly been employed for feedback control. However, the system dynamics encounters a significant resonance peak attributed to the lightly damped flexures, which restricts the control bandwidth to under 2% of the resonance frequency (Fleming (2009)). To address this constraint, inversion techniques such as notch filters are frequently used alongside tracking controllers to dampen resonant dynamics; thus increasing bandwidth (Feng et al. (2017)). However, deploying these filters necessitates a precise system model and is very sensitive to changes in system dynamics due to fluctuating payload mass. Active damping control has been explored and developed as an alternative, employing damping control within an inner feedback loop as part of a dual closed-loop framework (Chen et al. (2021)). Approaches like positive position feedback (PPF) (Moon et al. (2017)), integral resonant control (IRC) (Fleming et al. (2009)), etc., effectively dampen resonance with moderate tolerance to frequency variations. However, when integrated into an integral tracking loop, these systems face low gain margin constraints (Fleming (2009)). In general, the performance of contemporary damping controllers is limited because of the interdependence between gain and phase. Acknowledging this limitation, the authors have introduced and implemented a novel non-minimum phase resonant controller (NRC), which utilizes a constant-gain design with a tunable phase to dampen the resonant poles completely. This approach enables the attainment of bandwidths that exceed the system's resonance frequency within a dual closed-loop framework (Natu and HosseinNia (2024)).

⋆ This work was financed by Physik Instrumente (PI) SE & Co. KG and co-financed by Holland High Tech with PPS Project supplement for research and development in the field of High Tech Systems and Materials.

10.1016/j.ifacol.2025.10.166

Feedforward control, which involves dynamic system inversion, can be combined with feedback to improve tracking by improving the transient response and bandwidth (van Zundert and Oomen (2018)). However, this method is susceptible to modeling errors and uncertainties in plant parameters (Gu et al. (2014)). In raster scanning, feedforward combined with damping feedback reduces sensitivity to resonance variations and improves tracking (Aphale et al. (2008)). Two-degree-of-freedom (2DOF) designs use feedforward with tracking feedback controllers: high gains of the feedback controller handle low-frequency piezoelectric nonlinearities and disturbances, while feedforward compensates for linear dynamics (Butterworth et al. (2011),Leang et al. (2009)). Feedforward boosts performance where plant uncertainty is less than its nominal magnitude (Clayton et al. (2009)). Nanopositioning systems often have non-minimum phase (NMP) zeros, destabilizing inversion-based dynamics. Approximate inversion techniques like Zero Phase Error Tracking Control (ZPETC), Zero Magnitude Error Tracking Control (ZMETC), etc., (Butterworth et al. (2012)) are utilized for stable performance. Two 2DOF architectures aid this: feedforward plant-injection (FFPI) and feedforward closed-loop-injection (FFCLI) (Butterworth et al. (2009)). FFCLI is superior, as it simplifies the transfer function from the desired to the output position to a delay block and a low-order filter (Butterworth et al. (2010)). In AFM applications, perfectly delayed tracking is preferable if the delay is well known, though FFCLI's feedforward filter might become high-order to encompass the inverse dynamics of the closed-loop system (Butterworth et al. (2008)).

To date, there has been no recorded instance of a feedforward architecture that concurrently integrates both tracking and damping control. Furthermore, within dual closed-loop architectures, the plant inversion-based feedforward is insufficient for fulfilling the control objectives and is not interchangeable with closed-loop inversion feedforward, as indicated by the extant literature on standard control architectures. Consequently, this paper contributes by proposing a feedforward inner closed-loop inversion architecture in conjunction with a dual closed-loop feedback control system incorporating active damping. The feedforward filter, developed based on the inversion of partial inner closed-loop dynamics, facilitates the precise delayed tracking of reference signals. This architecture utilizes a unity-gain shaping filter, effectively minimizing the real feedback error attributable to reference inputs. In addition, the paper presents a simulated case study employing a simplified dynamic model of an industrial nanopositioning system to illustrate enhancements in closed-loop reference tracking performance within the bandwidth frequency regime.

The paper is organized as follows: Section 2 explains the control architecture, objectives, and limitations of plant inversion-based feedforward control, and presents the design principles for the proposed method. Section 3 applies the method in a simulated case study involving simplified nanopositioner dynamics. Section 4 presents time-domain reference tracking results. Section 5 concludes the paper and suggests future work.

2. COMBINED FEEDFORWARD & INPUT SHAPING

2.1 Control Architecture

Fig. 1 shows the control framework with a feedforward controller $F_f(s)$ and input shaping filter $F_s(s)$ within a dual closed-loop architecture, integrating a tracking controller $C_t(s)$ and an active damping controller $C_d(s)$ for precise high-bandwidth control of nanopositioner dynamics $G(s)$.

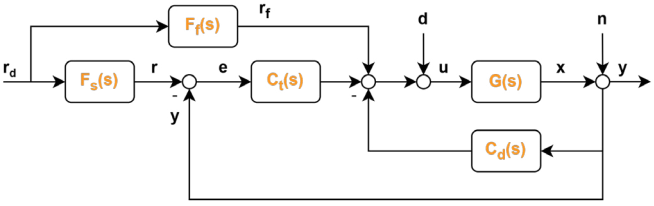

Fig. 1. Control architecture combining feedforward and input shaping with dual closed-loop feedback control.

The primary aim of this control framework is to facilitate accurate tracking of the desired reference r_d, while attenuating the impact of disturbances d and noise n on system performance. The measured output position y can be articulated in relation to the three inputs of the system:

$$y = \left(\frac{G(s)F_f(s) + G(s)C_t(s)F_s(s)}{1 + G(s)(C_t(s) + C_d(s))}\right) r_d + \left(\frac{G(s)}{1 + G(s)(C_t(s) + C_d(s))}\right) d + \left(\frac{1}{1 + G(s)(C_t(s) + C_d(s))}\right) n. \quad (1)$$

As demonstrated in (1), the contributions of $F_f(s)$ and $F_s(s)$ are confined to sensitivities associated with reference inputs, whereas the attenuation of disturbances and noise is independently addressed by the feedback controllers $C_t(s)$ and $C_d(s)$. The dynamics of the nanopositioning system can be expressed as:

$$G(s) = G_l(s)D(s), \quad (2)$$

where $G_l(s)$ denotes the linear system dynamics due to resonant modes and amplifier dynamics, and $D(s) = e^{-\tau s}$ accounts for the system's time delay τ.

The key considerations for implementing $F_f(s)$ and $F_s(s)$ in the control architecture in Fig. 1 are as follows:

- In nanopositioning systems, the strictly proper nature of plant $G(s)$ makes the inverse non-realizable, requiring taming for realization. Additionally, NMP zeros or delay in $G(s)$ may destabilize the inverse, requiring causal or non-causal methods for stability.
- The intended feedforward objective necessitates $y = r_d$, while the integrated control framework is applied to the actual setpoint feed r, thereby explicitly realizing the objective $y = r$. This aligns with the common aim of minimizing the tracking error $e = r - y$. Hence, it is essential to ensure that $F_s(s)$ does not alter the reference frequency components, necessitating $|F_s(s)| = 1$. Furthermore, delay compensation in $F_s(s)$ is employed consistently in practical applications, implying r_d is fed prior to r in the system.

2.2 Inadequacy of Plant Inversion-Based Feedforward

The feedforward control design is typically based on the inversion of the plant dynamics in standard control architectures. However, when active damping is integrated within the dual closed-loop framework, such plant inversion is inadequate to attain the feedforward goal. The following analysis supports this statement, where the feedforward filter is designed as follows:

$$F_f(s) = G_l^{-1}(s)F_t(s), \tag{3}$$

where $F_t(s)$ is the taming filter to make the inverse realizable. The objective is to minimize the sensitivity relating from the setpoint reference r to tracking error e, formulated as:

$$\frac{e}{r} = \frac{F_s(s)(1+G(s)C_d(s)) - G(s)F_f(s)}{F_s(s)(1+G(s)(C_t(s)+C_d(s)))}. \tag{4}$$

Substituting (3) into (4), and computing $F_s(s)$ for $e = 0$ gives:

$$F_s(s) = \frac{D(s)F_t(s)}{1+G(s)C_d(s)}. \tag{5}$$

Substituting (5) into (1) renders:

$$\frac{y}{r_d} = T_{yr_d}(s) = F_s(s) \neq 1. \tag{6}$$

Consequently, utilizing the plant inverse to design $F_f(s)$ does not facilitate perfect tracking of the intended reference. Additionally, it modifies the setpoint reference utilized by the feedback controllers, which is considered undesirable, as highlighted in the preceding subsection. This paves the way for designing feedforward control using inner closed-loop inversion, detailed in the next subsection.

2.3 Feedforward Inner-Closed-Loop-Inversion Architecture

In this subsection, we introduce a feedforward design based on inner closed-loop inversion, which facilitates the feedforward objectives of accurate reference tracking ($y = r_d$) and minimizing error ($e = 0$). The inner closed-loop dynamics $G_d(s)$ shaped utilizing an active damping controller $C_d(s)$ in feedback with plant $G(s)$ is given as:

$$G_d(s) = \frac{G(s)}{1+G(s)C_d(s)}. \tag{7}$$

Given that $G(s)$ encompasses a delay term $D(s)$, performing a direct inversion of $G_d(s)$ results in instability. To mitigate this issue, a causal approach is proposed, employing an inversion of partial inner closed-loop dynamics $G_d^*(s)$ to guarantee stability, given as:

$$G_d^*(s) = \frac{G_l(s)}{1+G(s)C_d(s)}. \tag{8}$$

The feedforward controller $F_f(s)$ can then be designed as:

$$F_f(s) = G_d^{*^{-1}}(s) \cdot F_t(s). \tag{9}$$

Here, $F_t(s)$ denotes the taming filter, which is defined by its low-pass characteristics, enabling the realizability of inversion, as given by:

$$F_t(s) = \left(\frac{\omega_t^2}{s^2 + 2\zeta_t\omega_t s + \omega_t^2}\right)^m, \tag{10}$$

where ω_t and ζ_t are the low-pass corner frequency and damping coefficient of the filter, respectively, and m is the order of the filter, chosen to be greater than the relative degree of $G_d^*(s)$.

In practice, careful selection of ω_t is crucial to avoid actuator saturation by keeping the control signal u below the saturation voltage threshold u_s. Considering the maximum reference signal $r_{d_{\max}}$ and control sensitivity $S_{ur_d}(s)$ ($r_d \mapsto u$), ω_t can be determined as:

$$\max \omega_t \,|\, \|S_{ur_d}(s)\|_\infty \cdot |r_{d_{\max}}| < |u_s|. \tag{11}$$

The feedforward $F_f(s)$ in (9) is designed to minimize error e. Using (4) and (9), the error sensitivity simplifies to:

$$\frac{e}{r} = \frac{F_s(s) - D(s)F_t(s)}{F_s(s)(1+G(s)(C_t(s)+C_d(s)))}. \tag{12}$$

Thus, to ensure $e = 0$, the shaping filter $F_s(s)$ should be:

$$F_s(s) = D(s)F_t(s). \tag{13}$$

Substituting (13) into (1), we get:

$$\frac{y}{r_d} = T_{yr_d}(s) = F_s(s), \tag{14}$$

where, $|F_s(s)| = 1 \;\forall\; \omega < \omega_t$. If ω_t is greater than the dual closed-loop bandwidth ω_c, characterized by the ± 3 dB bounds of $T_{yr_d}(s)$, then the proposed feedforward and input shaping methodology improves the tracking performance compared to the feedback-only case and achieves perfectly delayed tracking up to ω_c.

However, achieving a sufficiently high ω_t may not always be feasible in practical scenarios, thus affecting the tracking performance within the bandwidth frequency domain and, consequently, filtering out the reference ($r_d \neq r$). In such circumstances, it becomes necessary to re-tune $F_s(s)$ to a delay approximation $D'(s)$ ($F_s(s) = D'(s)$), such that:

$$\begin{aligned} |D'(s)| &= 1 && \forall\, \omega \in (0, \infty), \\ \angle D'(s) &= \angle D(s) + \angle F_t(s) && \forall\, \omega \in (0, \omega_c]. \end{aligned} \tag{15}$$

Thus, the proposed methodology achieves perfectly delayed tracking performance, fulfilling the objectives.

3. SIMULATED CASE STUDY

3.1 Nanopositioning System Dynamics

Presented in Fig. 2, the experimental setup utilizes a commercial P-621.1CD PIHera linear precision nanopositioner with a travel range of 100 μm. The single-axis positioning

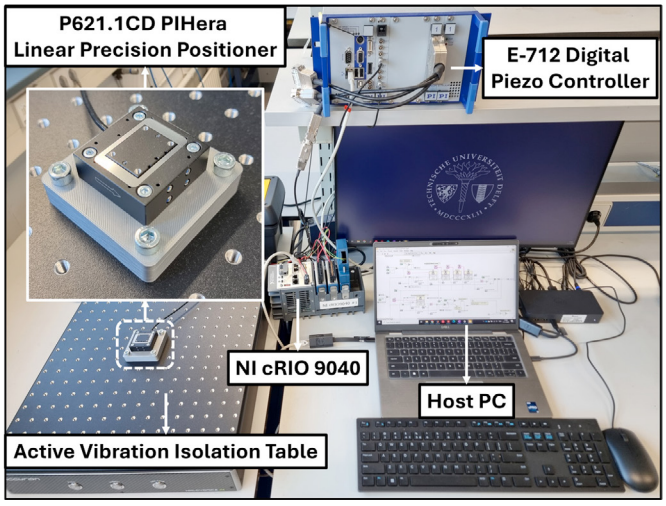

Fig. 2. Experimental setup utilized for identification of nanopositioning system from Physik Instrumente.

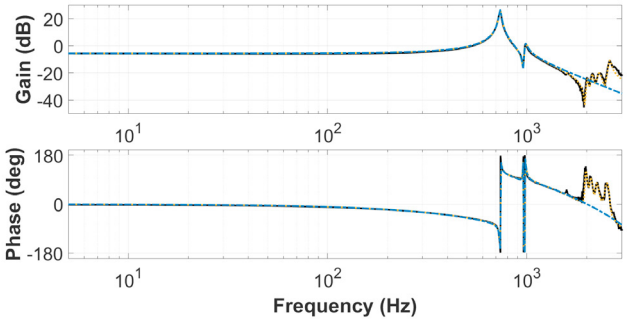

Fig. 3. Experimentally identified frequency response (——), 14th-order estimated system dynamics with delay (·····), and 6th-order estimated system dynamics with delay (-·-·).

stage incorporates a ceramic-insulated multilayer piezo-stack actuator, a flexure-based mechanism-guided platform, and a high-resolution capacitive sensor.

A sinusoidal chirp signal (0 to 0.1 V) was generated with LabVIEW and sent to the piezo-actuator for system identification. The capacitive sensor measured the position output, and the input-output signals were imported into MATLAB for analysis. The transfer functions were estimated using MATLAB's signal processing toolbox. A high sampling frequency F_s of $33.\overline{33}$ kHz provided sufficient data for an accurate identification.

The dominant resonance peak ω_n is at 735 Hz, with the second mode ω_2 nearby at 983 Hz (see Fig. 3). A notable phase delay occurs due to actuator-amplifier dynamics and system time delay, even at frequencies below ω_n. Higher modes appear around and beyond 2000 Hz. Pole-zero interlacing indicates the system's collocated nature.

For the simulated case study, a 6th-order transfer function inclusive of delay is estimated to adequately represent the predominant system dynamics, as derived from the identified frequency response (see Fig. 3).

$$G(s) = \frac{a_3 s^3 + a_2 s^2 + a_1 s + a_0}{b_6 s^6 + b_5 s^5 + b_4 s^4 + b_3 s^3 + b_2 s^2 + b_1 s + b_0} e^{-\tau s}, \tag{16}$$

where, $a_3 = 1.219\text{e}11$, $a_2 = 7.748\text{e}14$, $a_1 = 4.472\text{e}18$, $a_0 = 2.775\text{e}22$, $b_6 = 1$, $b_5 = 1.647\text{e}4$, $b_4 = 1.291\text{e}8$, $b_3 = 9.879\text{e}11$, $b_2 = 4.813\text{e}15$, $b_1 = 1.364\text{e}19$, $b_0 = 5.3\text{e}22$, and $\tau = 0.00018$.

3.2 Dual Closed-Loop Feedback Control

A tracking controller $C_t(s)$ and an active damping controller $C_d(s)$ operate simultaneously within the dual closed-loop feedback control architecture to enable the suppression of vibrational dynamics and facilitate high control bandwidths. In this paper, to enable complete damping of resonant poles, we use the Non-Minimum-Phase Resonant Controller (NRC) as $C_d(s)$, described by the transfer function:

$$C_d(s) = k \cdot \left(\frac{s - \omega_a}{s + \omega_a} \right), \tag{17}$$

where $C_d(s) = k \, \forall \, \omega \in [0, \infty)$, and ω_a signifies the tunable corner frequency. The controller gain is tuned as $k = |G^{-1}(0)|$, to place a pole at $s = 0$, while the locus of the

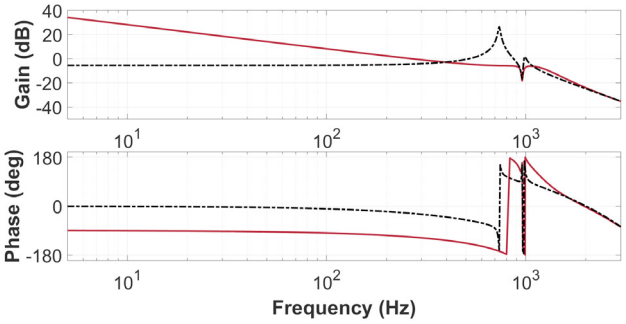

Fig. 4. Frequency response of estimated plant $G(s)$ (-·-·) and inner closed-loop $G_d(s)$ (——).

remaining two resonant poles varies with $\omega_a = n \cdot \omega_n$, where the normalized parameter n is tuned based on the required damping of the targeted and nearby resonant mode.

The inner closed-loop transfer function from the input disturbance d to the system output y, formulated as $G_d(s)$ in (7), is illustrated in Fig. 4. Here, for $n = 8$, the NRC completely dampens the dominant resonance mode while significantly damping the second mode.

The $C_t(s)$ in the outer loop is then designed based on $G_d(s)$ to achieve the highest possible ω_c, where a proportional-integral (PI) controller is employed to set the desired bandwidth and ensure zero steady-state error. A notch filter $N(s)$ is used in series to suppress the partially-damped second mode alongside a low-pass filter to attenuate high-frequency noise and unmodelled dynamics. The transfer function is represented as:

$$C_t(s) = \underbrace{k_p \left(1 + \frac{\omega_i}{s}\right)}_{\substack{\text{Proportional} \\ \text{Integral Term}}} \underbrace{\frac{\left(\frac{s}{\omega_N}\right)^2 + \frac{s}{Q_1 \omega_N} + 1}{\left(\frac{s}{\omega_N}\right)^2 + \frac{s}{Q_2 \omega_N} + 1}}_{\substack{\text{Notch} \\ \text{Filter}}} \underbrace{\left(\frac{\omega_l}{s + \omega_l}\right)}_{\substack{\text{Low-Pass} \\ \text{Filter}}}, \tag{18}$$

where, $k_p = 1.0533$, $\omega_i = 28$ Hz, $\omega_N = 1000$ Hz, $Q_1 = 1.1$, $Q_2 = 1$, $\omega_l = 3000$ Hz. Thus, the NRC and PI controllers in conjunction enable ω_c to be achieved beyond ω_n. $F_f(s)$ and $F_s(s)$ are designed using (9) and (13), with the filter $F_t(s)$ tuned to $\omega_t = 930$ Hz, $\zeta_t = 0.6$, and $m = 2$. Fig. 5 shows the frequency response comparison between the feedback-only and the combined feedback-feedforward architectures.

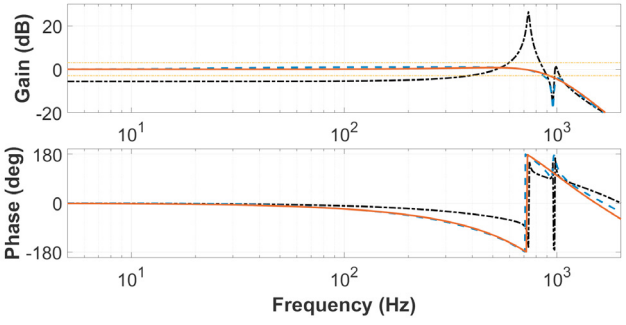

Fig. 5. Frequency response of plant $G(s)$ (-·-·), and dual closed-loop $T_{yr_d}(s)$ with feedback-only (——) and combined with feedforward (——), ±3 dB bounds (- - -).

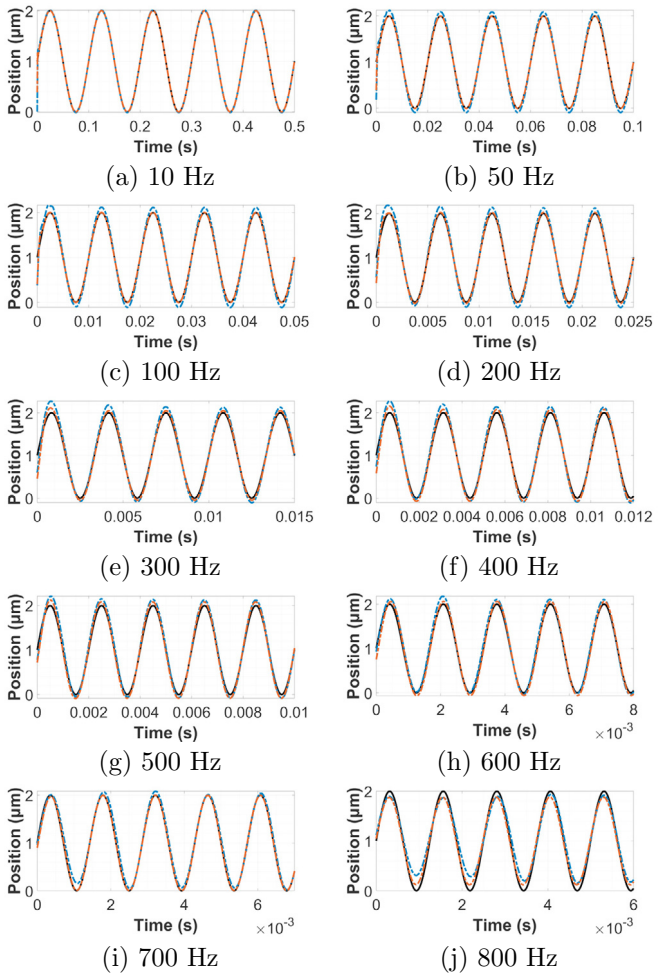

Fig. 6. Sinusoidal tracking performance with feedback-only (- - -) and combined with feedforward (- · -) for reference input (——) with different frequencies.

4. SIMULATED TRACKING PERFORMANCE

The nanopositioning stage aims to follow predefined trajectories, typically periodic ones, accurately. Fig. 5 demonstrates tracking up to dual closed-loop bandwidths ω_c in the frequency domain. This section assesses time-domain performance with sinusoidal references from 10 to 800 Hz.

Phase lag increases with frequency in dual closed-loop systems. Perfectly delayed tracking is used in periodic scanning when the delay is known. Post-processing techniques remove phase lags to represent tracking performance accurately. The known phase lag ϕ_l (degrees) at frequency f (Hz) is used to compute the time delay t_d.

$$t_d = \frac{\phi_l}{f \cdot 360}. \tag{19}$$

Subsequently, the shifted outputs $y^*(t)$ can be computed as follows:

$$y^*(t) = y(t_{i+N_d} : t_N) \text{ for } i = [1, N] \text{ and } i \in Z. \tag{20}$$

In discrete time, phase lags are compensated by shifting $N_d = \lfloor |t_d|/t_s \rceil$ samples, where t_s is the sampling time, and $\lfloor \cdot \rceil$ is the round function. Fig. 6 shows the phase-corrected system tracking response for small-amplitude sinusoidal references from 0 to 2 μm.

Table 1. RMS Tracking Errors

Frequency (Hz)	Feedback-only (μm)	Feedback-Feedforward (μm)
10	0.0250	0.0069
50	0.0656	0.0073
100	0.0814	0.0087
200	0.0852	0.0184
300	0.0849	0.0398
400	0.0847	0.0525
500	0.0728	0.0643
600	0.0561	0.0530
700	0.0382	0.0055
800	0.1090	0.0953

To assess the tracking performance of the dual closed-loop system with and without feedforward control, the root mean square tracking error (e_{rms}) index is considered, given as:

$$e_{rms} = \sqrt{\frac{1}{N}\sum_{i=1}^{N} \left(y\left(t_i\right) - r\left(t_i\right)\right)^2}, \tag{21}$$

where, $r(t_i)$ and $y(t_i)$ represents the reference signal and output signal at discrete time step i, respectively, and N is the total number of samples, with $i = 1, 2, 3, ..., N$.

Table 1 presents the calculated root mean square (RMS) tracking errors, both in the presence and absence of feedforward control. The results clearly indicate that the system sustains exceptionally low errors for both scenarios, with reference signal frequencies varying up to 800 Hz, which is approximately in agreement with ω_c. Notably, the architecture integrating the proposed feedforward and input-shaping design yields superior tracking performance compared to the feedback-only configuration, thereby demonstrating the efficacy of the proposed design methodology. Recognizing that these error magnitudes are subject to variation contingent upon the precise tuning of all controller parameters, which are adjusted according to specific application requirements, is crucial. The values presented exemplify the system's tracking capabilities up to ω_c.

5. CONCLUSIONS AND FUTURE WORK

This study addresses the limitations of traditional feedforward control approaches in dual closed-loop nanopositioning systems, where active damping is employed to mitigate lightly damped resonant dynamics. By introducing a feedforward architecture based on partial inner closed-loop dynamics inversion, the proposed framework overcomes the inadequacies of plant inversion-based feedforward strategies in such configurations. Integrating this feedforward filter with a unity-gain shaping filter effectively reduces reference-induced feedback errors, enabling precise, delayed tracking of reference signals within the bandwidth frequency regime. A simulated case study using a simplified industrial nanopositioning system model highlights the practical benefits of the approach, including enhanced tracking accuracy to periodic reference inputs. Future research can focus on experimental validation, robustness analysis under unmodeled dynamics, load variations, actuator nonlinearities and disturbances, and extension to multi-degree-of-freedom systems to expand the applicability of the proposed methodology.

ACKNOWLEDGEMENTS

The authors express their sincere gratitude to Mathias Winter, Head of Piezo System & Drive Technology, and Dr.-Ing. Simon Kapelke, Head of Piezo Fundamental Technology, for their invaluable collaboration in providing technical insights concerning the system and its applications.

REFERENCES

Aphale, S.S., Devasia, S., and Moheimani, S.R. (2008). High-bandwidth control of a piezoelectric nanopositioning stage in the presence of plant uncertainties. *Nanotechnology*, 19(12), 125503.

Butterworth, J.A., Pao, L.Y., and Abramovitch, D.Y. (2008). Architectures for tracking control in atomic force microscopes. *IFAC Proceedings Volumes*, 41(2), 8236–8250.

Butterworth, J.A., Pao, L.Y., and Abramovitch, D.Y. (2009). A comparison of control architectures for atomic force microscopes. *Asian Journal of Control*, 11(2), 175–181.

Butterworth, J.A., Pao, L.Y., and Abramovitch, D.Y. (2010). Adaptive-delay combined feedforward/feedback control for raster tracking with applications to afms. In *Proceedings of the 2010 American Control Conference*, 5738–5744. IEEE.

Butterworth, J.A., Pao, L.Y., and Abramovitch, D.Y. (2011). A discrete-time single-parameter combined feedforward/feedback adaptive-delay algorithm with applications to piezo-based raster tracking. *IEEE transactions on control systems technology*, 20(2), 416–423.

Butterworth, J.A., Pao, L.Y., and Abramovitch, D.Y. (2012). Analysis and comparison of three discrete-time feedforward model-inverse control techniques for nonminimum-phase systems. *Mechatronics*, 22(5), 577–587.

Chen, Z., Zhong, X., Shi, J., and Zhang, X. (2021). Damping-enabling technologies for broadband control of piezo-stages: A survey. *Annual Reviews in Control*, 52, 120–134.

Clayton, G.M., Tien, S., Leang, K.K., Zou, Q., and Devasia, S. (2009). A review of feedforward control approaches in nanopositioning for high-speed spm.

Devasia, S., Eleftheriou, E., and Moheimani, S.R. (2007). A survey of control issues in nanopositioning. *IEEE Transactions on Control Systems Technology*, 15(5), 802–823.

Feng, Z., Ling, J., Ming, M., and Xiao, X.H. (2017). High-bandwidth and flexible tracking control for precision motion with application to a piezo nanopositioner. *Review of Scientific Instruments*, 88(8).

Fleming, A.J. (2009). Nanopositioning system with force feedback for high-performance tracking and vibration control. *IEEE/Asme Transactions on Mechatronics*, 15(3), 433–447.

Fleming, A.J., Aphale, S.S., and Moheimani, S.R. (2009). A new method for robust damping and tracking control of scanning probe microscope positioning stages. *IEEE Transactions on nanotechnology*, 9(4), 438–448.

Fleming, A.J. and Leang, K.K. (2014). *Design, modeling and control of nanopositioning systems*. Springer.

Gu, G.Y., Zhu, L.M., Su, C.Y., Ding, H., and Fatikow, S. (2014). Modeling and control of piezo-actuated nanopositioning stages: A survey. *IEEE Transactions on Automation Science and Engineering*, 13(1), 313–332.

Leang, K.K., Zou, Q., and Devasia, S. (2009). Feedforward control of piezoactuators in atomic force microscope systems. *IEEE Control Systems Magazine*, 29(1), 70–82.

Moon, R.J., San-Millan, A., Aleyaasin, M., Feliu, V., and Aphale, S.S. (2017). Selection of positive position feedback controllers for damping and precision positioning applications. In *Modeling, Design and Simulation of Systems: 17th Asia Simulation Conference, AsiaSim 2017, Melaka, Malaysia, August 27–29, 2017, Proceedings, Part I 17*, 289–301. Springer.

Natu, A.M. and HosseinNia, S.H. (2024). Non-minimum-phase resonant controller for active damping control: Application to piezo-actuated nanopositioning system. URL `https://arxiv.org/abs/2412.18374`.

Shan, Y. and Leang, K.K. (2013). Design and control for high-speed nanopositioning: Serial-kinematic nanopositioners and repetitive control for nanofabrication. *IEEE Control Systems Magazine*, 33(6), 86–105. doi:10.1109/MCS.2013.2279474.

van Zundert, J. and Oomen, T. (2018). On inversion-based approaches for feedforward and ilc. *Mechatronics*, 50, 282–291.